11th ANKARA INTERNATIONAL AEROSPACE CONFERENCE **AIAC-2021-071**
8-10 September 2021 - METU, Ankara TURKEY

LARGE EDDY SIMULATION OF A TRIANGULAR BLUFF BODY USING AN IN-HOUSE FLOW SOLVER

Omer Yalili*, Tamer Sener†, Mustafa Sengul‡, Kadri Kocer§, and Ayse G. Gungor¶
Faculty of Aeronautics and Astronautics, Istanbul Technical University
Istanbul, Turkey

ABSTRACT

This study aims to demonstrate the capabilities of an in-house large eddy simulation (LES) flow solver, lestr3d, for flows with complex features, such as separation, vortex shedding and wall-vortex interaction. The case that is presented in this study is the flow around a triangular bluff body with the objective of evaluating the solver's capability as used to simulate this simple design with complex flow features, for which detailed measurements exist on a comparison basis. Three-dimensional flow is simulated using different sgs models, including Smagorinsky, k-equation, and wall-adaptive local eddy viscosity (WALE) model. Wall-bounded LES simulations for the Volvo bluff body are performed with 46000 Reynolds number. In the analysis, root mean square (rms) velocities and wall-normal direction comparison for different mesh resolution and experimental data, and mean axial velocity contours, normalized rms axial velocity contours and anisotropy distributions for Smagorinsky, k-equation and WALE sgs models are shown. Results of this study indicates that most of the outcomes of the numerical solution are compatible with the experimental data.

INTRODUCTION

Turbulent flows; as in many parts of nature, are common in aerospace industry. Even though it is very common and has been investigated for many years, the mystery of turbulence has not yet been completely solved. The chaotic, nonlinear, and multi-scale nature of turbulence makes it difficult to know all the details about it. It is not possible to define turbulence precisely and completely; however, the characteristic features of turbulent flows can be understood [Tennekes and Lumley, 1972; Ecke, 2005].

Understanding and analyzing turbulent flows are crucial in engineering applications and scientific research. With the development of computer science, computational fluid dynamics (CFD) are widely used to study the spatial and temporal dynamics of complex, three-dimensional turbulent flows. There are three main approaches used in the study of CFD: direct numerical simulation

*BSc. Student in Aero. and Astro. Eng., Email: yalili@itu.edu.tr
†PhD. Student in Aero. and Astro. Eng, Email: senerta@itu.edu.tr
‡PhD. Student in Aero. and Astro. Eng, Email: sengulmu@itu.edu.tr
§MSc. Student in Aero. and Astro. Eng, Email: kocer20@itu.edu.tr
¶Assoc. Prof, Email: ayse.gungor@itu.edu.tr

(DNS), Reynolds-averaged Navier-Stokes (RANS), and large eddy simulation (LES). Turbulence features a wide variety of characteristic length and time scales. DNS is the method that solves all the scales from the largest to the smallest. The capabilities of current computer technologies limit the DNS of complex turbulent flows at high Reynolds numbers [Lacaze and Oefelein, 2015]. RANS equations are the governing equations for the time-averaged fluid motion. It is obtained by decomposing the instantaneous values of variables into their mean and fluctuations about their mean value. Hence, RANS approach, on the other hand is feasible for high Reynolds number flows but appears to be insufficient to meet the growing design principles of the aerospace industry. LES approach uses a spatial filter to cut out turbulent structures associated with length scales smaller than the filter length. This filter is a low pass filter. Small turbulent structures are filtered out, thus reducing the grid resolution requirements encountered in DNS. Sub-grid scale (sgs) models are used to account for the effects of filtered small-scale structures. In between the high cost of DNS and the low resolution of RANS, LES appears to be a suitable approach to analyze turbulence dynamics widely used in aerospace industry today [Andersson et al, 2015; Falese et al, 2014; Gourdain et al, 2009b]. CFD solvers using these approaches can be classified into two main categories: commercial and opensource. Day by day, the use of opensource softwares are increasing both in industry and academia.

This study aims to improve the capability of our in-house LES solver, $lestr3d$, which is benchmarked before [Karahan et al, 2017]. This will be accomplished by analyzing three dimensional turbulent flow around a triangular bluff body commonly encountered in aerospace applications.

Firstly, the governing equations and sub-grid scale models required to close these equations are presented. Then, the software details and the numerical methods used are explained. Subsequently, comparative results of LES of the flow around the Volvo bluff body using $lestr3d$ obtained with Samagorinsky, k-equation, wall-adapting local eddy-viscosity (WALE) sgs models are presented. Further studies are discussed in the last section.

GOVERNING EQUATIONS

LES equations are obtained by filtering spatially Navier Stokes equations. Thus, large scales are solved and small scales are modelled. This filter can be defined in general terms with a kernel filter as follows:

$$\overline{u}_i(x,t) \;=\; \int G(x,-\xi;\;\overline{\Delta})\;u_i(\xi,t)d\xi.$$

Where, filtering holds u_i values occurring at scales larger than in filter width Δ. Basically, the filter function G equates u_i values that occur on small scales to zero. Navier-Stokes equations are filtered and the scales to be modeled are separated from those to be calculated directly. In this study, top-hat filter is used as defined:

$$G(x-\xi) \;=\; \begin{cases} \dfrac{1}{\overline{\Delta}} & if|x-\xi| \leq \dfrac{\overline{\Delta}}{2} \\ 0 & \text{otherwise} \end{cases}$$

In LES, filtering is actualized by Leonard decomposition. With this decomposition, the turbulent flow is divided into a large scale and a small scale. The large-scale component is filtered term $\overline{u}_i$. The small-scale component (sub-grid scale, sgs) is fluctuating $u_i^{'}$. Favre filter (density based filter) is used to prevent the emergence of sgs terms in the continuity equation in compressible flows. Favre filter:

$$\tilde{\Psi} \;=\; \frac{\overline{\rho\Psi}}{\overline{\rho}} \;\rightarrow\; \overline{\rho\Psi} \;=\; \overline{\rho}\tilde{\Psi}$$

$$\overline{\rho\Phi\Psi} \;=\; \overline{\rho}\tilde{\Phi}\tilde{\Psi} \;+\; \overline{\rho}(\widetilde{\Phi\Psi} - \tilde{\Phi}\tilde{\Psi})$$

Applying Favre-filter and box filter to Navier Stokes equations, compressible LES governing equations for continuity, momentum, and total energy are as follows, respectively;

$$\frac{\partial\overline{\rho}}{\partial t} + \frac{\partial\overline{\rho}\tilde{u}_i}{\partial x_i} = 0; \tag{1}$$

$$\frac{\partial\overline{\rho}\tilde{u}_i}{\partial t} + \frac{\partial}{\partial x_j}[\overline{\rho}\tilde{u}_i\tilde{u}_j + \overline{p}\delta_{ij} - \tilde{\tau}_{ij} + \tau_{ij}^{sgs}] = 0; \tag{2}$$

$$\frac{\partial\overline{\rho}\tilde{E}}{\partial t} + \frac{\partial}{\partial x_i}[(\overline{\rho}\tilde{E} + \overline{p})\tilde{u}_i + \tilde{q}_i - \tilde{u}_j\tilde{\tau}_{ij} + H_i^{sgs}] = 0, \quad i,j = 1,2,3. \tag{3}$$

In these equations, i and j are Einstein's summation convention indices, t is time, $x_{i,j}$ is spatial coordinates, $\tilde{u}_{i,j}$ is velocity, $\overline{p}$ is pressure, $\tilde{\tau}_{ij}$ and τ_{ij}^{sgs} are stress tensors in main flow and subgrid-scale, $\tilde{E}$ is energy, $\tilde{q}_i$ is heat flux, and H_i^{sgs} is sgs enthalpy flux.

In LES equations, the subgrid stress tensor needs to be modelled. The Boussinesq Hypothesis [Pope, 2001; Sagaut, 2006] is a widely used approach for modeling sgs terms. In this study, three different sgs models which are Smagorinsky model [Erlebacher et al, 1992], k-equation model [Yoshizawa and Horiuti, 1985] and wall adapting local eddy viscosity (WALE) model [Nicoud and Ducros, 1999] are used. Smagorinsky model is a zero-equation model. The extended version of the Smagorinsky model for compressible flow. It is a zero-equation model and the equation for compressible flow is associated with the strain rate in the flow area. Stresses are calculated using velocities from solution domain. k-equation model, called one-equation model, is a model that calculates sgs turbulent kinetic energy (TKE) by solving an additional differential equation. This model considers history and spatial effects when we compare with Smagorinsky model. The WALE model calculates the eddy viscosity value using the symmetrical part of the square of the velocity gradient tensor. In the Smagorinsky model, sgs dissipation overestimates because when the wall goes to zero, sgs viscosity does not go to zero. Correct scaling behaviour is acquired close to the wall in the WALE sgs model.

NUMERICAL METHOD

The in-house LES solver, is a compressible flow solver written in FORTRAN and relies on Message-Passing Interface (MPI) libraries for parallel applications. In addition, domain decomposition is performed using METIS software.

The numerical method used in *lestr3d* is the finite volume method (FVM). The FVM formulation of the compressible LES equations in integral form can be written as;

$$\frac{\partial}{\partial t}\int_\Omega \vec{Q}\mathrm{d}\Omega + \oint_S (\vec{F}_c - \vec{F}_v - \vec{F}^{sgs})\mathrm{d}S = \Phi^{sgs}. \tag{4}$$

Conservative flux vector ($\vec{Q}$) is being stored at the cell center for each volume is given as;

$$\vec{Q} = \begin{bmatrix}\overline{\rho} & \overline{\rho}\tilde{u} & \overline{\rho}\tilde{v} & \overline{\rho}\tilde{w} & \overline{\rho}\tilde{E} & \overline{\rho}\tilde{k}\end{bmatrix}^T.$$

There are also other vectors in addition to the conservative flux vector. These are convective, viscous and sgs flux vectors ($\vec{F}_c$, $\vec{F}_v$, $\vec{F}^{sgs}$) can be written respectively as;

$$\vec{F}_c = \begin{bmatrix}\overline{\rho}V \\ \overline{\rho}\tilde{u}V + n_x\overline{p} \\ \overline{\rho}\tilde{v}V + n_y\overline{p} \\ \overline{\rho}\tilde{w}V + n_z\overline{p} \\ (\overline{\rho}\tilde{E} + \overline{p})V \\ \overline{\rho}\tilde{k}V\end{bmatrix}, \quad \vec{F}_v = \begin{bmatrix}0 \\ n_x\tilde{\tau}_{xx} + n_y\tilde{\tau}_{xy} + n_z\tilde{\tau}_{xz} \\ n_x\tilde{\tau}_{yx} + n_y\tilde{\tau}_{yy} + n_z\tilde{\tau}_{yz} \\ n_x\tilde{\tau}_{zx} + n_y\tilde{\tau}_{zy} + n_z\tilde{\tau}_{zz} \\ n_x\tilde{\Theta}_x + n_y\tilde{\Theta}_y + n_z\tilde{\Theta}_z \\ 0\end{bmatrix}, \quad \vec{F}^{sgs} = \begin{bmatrix}0 \\ n_x\tau_{xx}^{sgs^\circ} + n_y\tau_{xy}^{sgs^\circ} + n_z\tau_{xz}^{sgs^\circ} \\ n_x\tau_{yx}^{sgs^\circ} + n_y\tau_{yy}^{sgs^\circ} + n_z\tau_{yz}^{sgs^\circ} \\ n_x\tau_{zx}^{sgs^\circ} + n_y\tau_{zy}^{sgs^\circ} + n_z\tau_{zz}^{sgs^\circ} \\ n_xH_x^{sgs^\circ} + n_yH_y^{sgs^\circ} + n_zH_z^{sgs^\circ} \\ \frac{\mu_t}{Pr_t}\left(\frac{\partial\tilde{k}}{\partial x} + \frac{\partial\tilde{k}}{\partial y} + \frac{\partial\tilde{k}}{\partial z}\right)\end{bmatrix}.$$

LES equations are discretized on grids and for spatial discretization the second-order central scheme is used. Jameson-Schmidt-Turkel artificial dissipation scheme is implemented to the code for prevent numerical oscillations due to central scheme. A five-stage Runge-Kutta scheme is used for explicit-time integration. The application of boundary conditions is performed with ghost cell methodology. More detailed information about the numerical accuracy, scalability up to 896 cores and capability of the solver for turbulent wall-bounded flows are given in [Karahan, 2017; Er, 2019].

VOLVO BLUFF BODY PROBLEM

It is very important to maintain sustainable combustion in systems where the air-fuel flows velocity exceeds the normal burning velocity. In these systems, the device that maintains the flame and provides stability is called bluff body. The Bluff body enables the generation of periodic vortexes that act as flame stabilizers. Thus, analyzing bluff bodies in aerospace industry is very crucial. In this study, this problem is chosen to evaluate the solver's capability to simulate this design with complex flow features, for which detailed measurements and numerical studies exist.

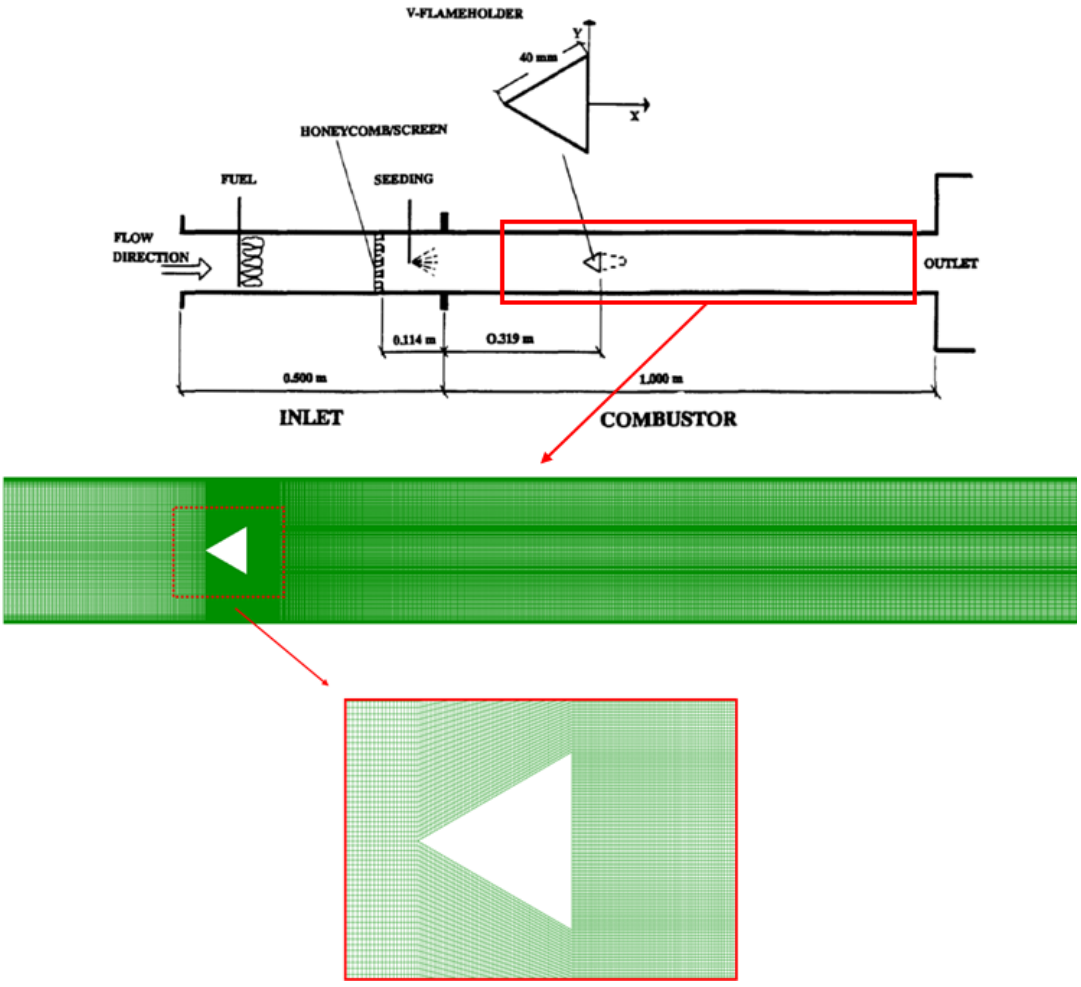

Figure 1: A schematic drawing of the experimental setup [Sjunnesson et al, 1992]. Red-framed area shows the solution domain. The grid structure created for this region is in the bottom with a zoomed view around the bluff body.

A schematic drawing of the Volvo experimental setup [Sjunnesson et al, 1992] is shown in Figure 1. Note that, the computational domain only focuses on the region that is depicted in the figure. This choice of the domain size, details are given in Table 1 is in agreement with other numerical studies. TThe computational domain is discretized with 4.9 million hexahedral elements and 1 million

hexahedral elements. The coarser mesh is used in order to see the effect of the mesh resolutions on the results and reduce computational cost in the computational domain. The coarse mesh has a coarser structure than the fine mesh, especially in the z direction. The capture the flow details accurately, mesh is stretched near walls and the wake region. The two-dimensional mesh in the mid-plane is also presented in Figure 1.

Table 1: Geometrical details

Properties	Value	Dimension
Length of channel	0.882	[m]
Height of channel	0.12	[m]
Depth of channel	0.08	[m]
Length of the bluff body	0.04	[m]
The location of the bluff body	0.2	[m]
Bluff body angle	60	[°]
Inlet flow angle	0	[°]
Outlet flow angle	0	[°]

Periodic boundary condition was defined to the front and back surfaces. No-slip adiabatic boundary condition was assigned to upper, lower and prism wall surfaces; simple input and simple output boundary conditions were applied to the inlet and outlet.

RESULTS

Volvo bluff body analysis was performed in $lestr3d$ code with Smagorinsky, k-equation and WALE subgrid scale (sgs) models. Smagorinsky and WALE sgs simulations were run using 84 and 28 cores respectively in the National Center for High Performance Computing (UHeM) of Turkey, and the k-equation subgrid model simulation was run using 18 cores at the local server $Vortex$.

The uniform inflow velocity is $U = 16.6m/s$. Reynolds number based on the length of the bluff body and inflow velocity is $Re = 46000$. The statistics are collected for 17 flow through times (FTT) with Smagorinsky model, 6 FTT with k-equation model, 8.5 FTT with WALE model after an initial washout of 6 FTT. FFT can be calculated as; $\tau_b = L/u_{inlet}$. Here L is the streamwise length of the computational domain and u_{inlet} is the inflow velocity.

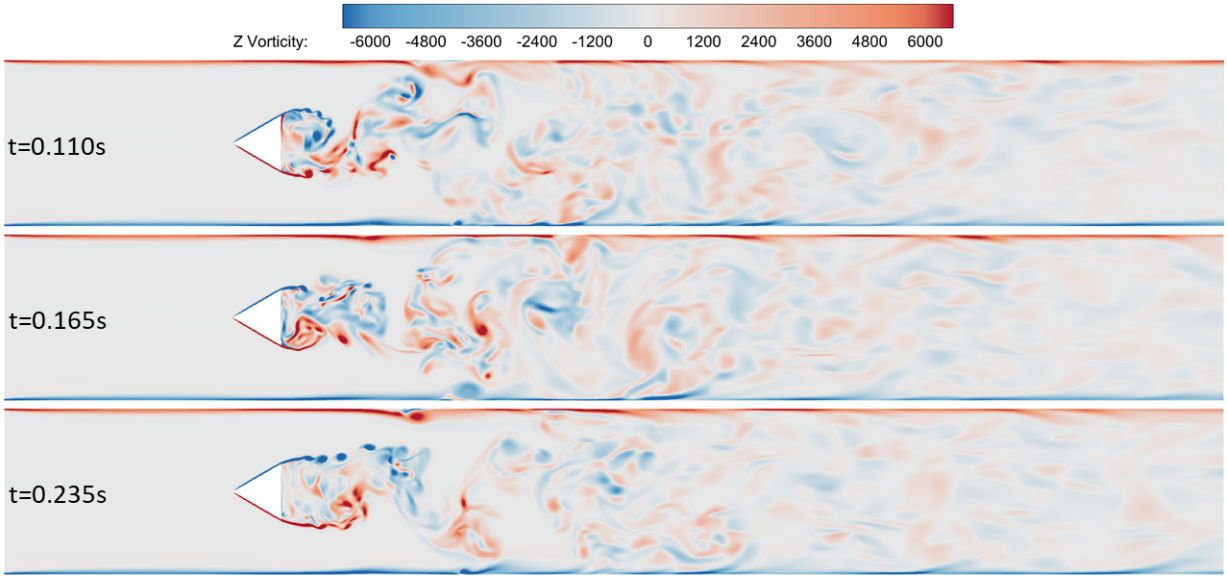

Figure 2: Instantaneous spanwise vorticiy contours at three different instants at the mid plane.

Unsteady Flow Features

The instantaneous spanwise vorticity contours are shown for three different instants in Figure 2 for the Smagorinsky model. Results demonstrate qualitatively correct development of the vortical structures, which are populated by strong antipole vortices due to the vortex shedding at the re-circulation region and intense three-dimensional vortices downstream. Moreover, the wall-vortex interaction, which plays a significant role in the spatial development of the bluff-body induced vortex shedding mechanism, and hence for stabilizing the flame in reacting flows [Doligalski et al, 1994] is seen to be well captured. These preliminary instantaneous realizations of the flow around a bluff body present the predictive capability of the in-house solver for flows with complex flow features, such as separation, vortex shedding and wall-vortex interaction. Figure 3 presents the illustration of the coherent structures obtained from the Q criterion colored by instantaneous axial velocity.

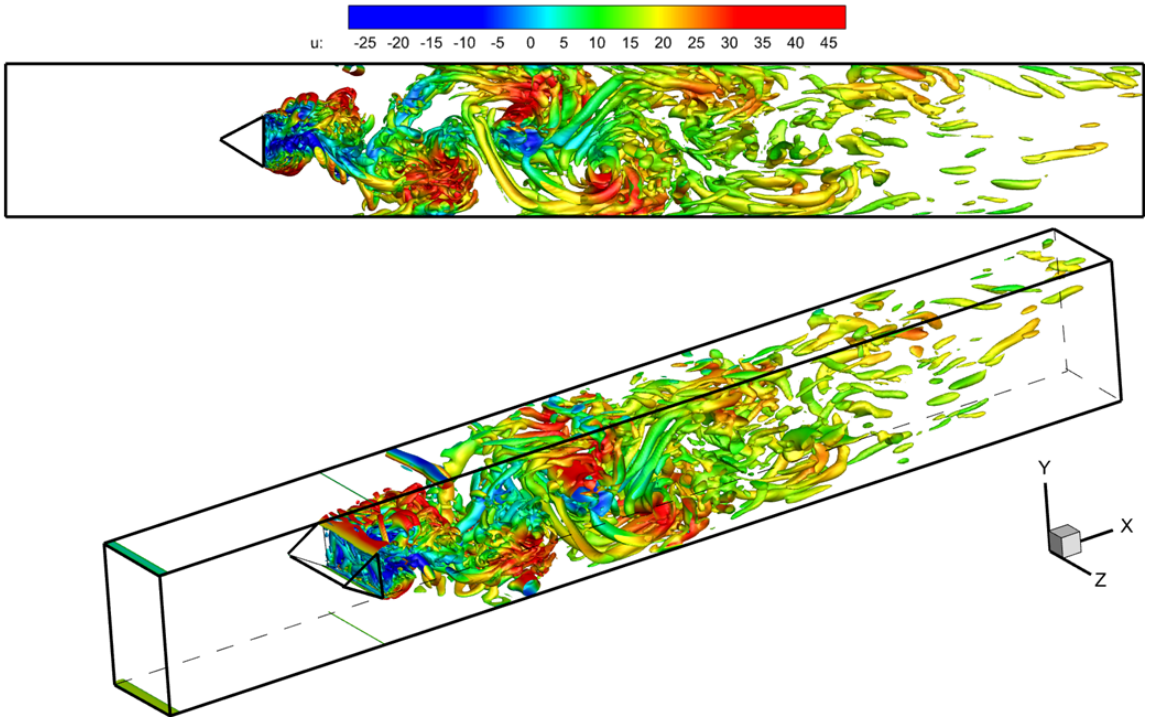

Figure 3: Instantaneous visualization of Q structures. Top side view, bottom 3D view.

Statistics

To test the accuracy of the simulation, a probe was placed just behind the bluff body. The received data were analyzed by Fast Fourier Transform (FFT). Probe data were taken from the simulation with Smagorinsky, k-equation, and WALE sgs models and analyzed.

The shedding frequency is found with the data obtained from the probes and the Strouhal number is calculated. Table 2 presents the LES and experimental results [Sjunnesson et al, 1992; Giacomazzi et al, 2004] in terms of vortex shedding frequency and Strouhal number. According to this table, LES results are in good agreement with the experimental results for all sgs models.

Table 2: Comparison of experimental and LES statistics.

	Vortex Shedding Frequency [1/s]	Strouhal Number
LES with Smag.	124.87	0.30
LES with k-eq	125	0.30
LES with WALE	116	0.28
Experiments	105	0.25

Time-averaged statistics are collected every 25 time-steps (sampling frequency) over 17 FTT times

with Smagorinsky, 6 FTT times with k-equation, and 8.5 FTT times with WALE sgs model. All velocities are normalized to the bulk velocity value ($Ubulk = 16.6m/s$) and all lengths are normalized to the bluff body characteristic length ($x/D = 0.04m$). Results are compared with the experimental results of Wu et al.(2017).

The time-averaged velocities behind the bluff body are investigated in five different sections. These sections are located at normalized distances of $x/D =$ 0.375 (a), 0.85 (b), 1.53 (c), 3.75 (d) and 9.4 (e). The point where the bluff body ends is considered as the origin.

Figure 4 shows a comparison of root mean square (rms) velocities in the axial direction calculated with coarse and fine mesh for Smagorinsky sgs model. Rms values are an important indicator in the measurement of varying amounts. Therefore, it also gives information about turbulence. The results obtained with the fine mesh in each plot agree with the experiment, while the results of the coarse mesh are quite inconsistent with the experimental data. Generally, higher velocities are calculated with the coarse mesh than the experimental data, and serious deviations are observed especially in the y/D=±0.5 region (lower and upper corners of the coarse body). High shear stress is expected in these regions, the coarse mesh did not solve these regions well. The results show that the coarse mesh is not suitable for this problem. Fine mesh will be used in subsequent analyzes and sgs model effects will be examined.

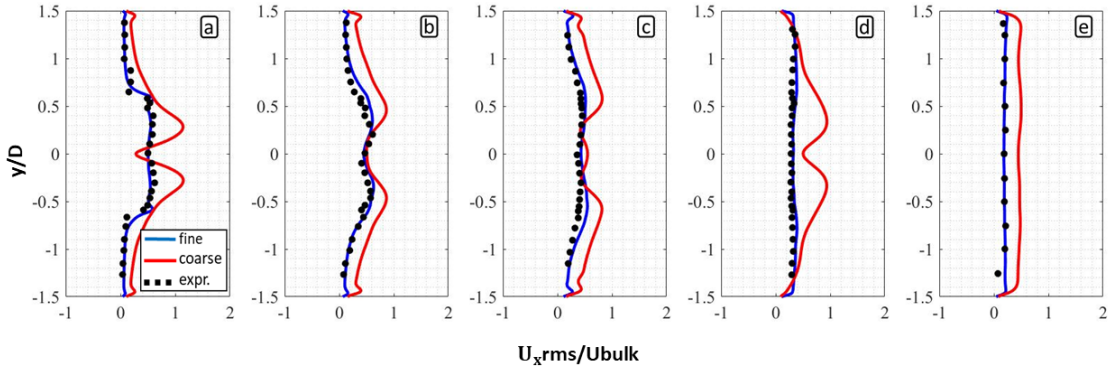

Figure 4: The rms axial velocity distribution on the centerline along the sample lines $x/D =$ 0.375 (a), 0.85 (b), 1.53 (c), 3.75 (d) and 9.4 (e) stations.

Figure 5 shows the mean velocity distribution and the anisotropy distribution on the centerline along the streamwise direction. The mean velocity distribution gives information about the recirculation region. In the recirculation region, mean axial velocity reaches a normalized velocity of -0.5 then reaches up to inlet velocity. As seen in the figure, the results obtained with the all sgs models are quite close to the experimental data. Moreover, it can be seen that the anisotropy predictions with all sgs models are compatible with the experimental data.

Figure 6 shows the mean streamwise distributions behind the bluff body over five control sections. The re-circulation region and the development of the flow behind the bluff body is captured accurately. Around the bluff body, flow is accelerated because of the blockage phenomenon. Behind the bluff body, highly turbulent region is observed and flow is driven by dense negative signed vortices which are generated by the corners of the bluff body. The wake effect is disappeared towards to the outlet region and the axial velocity profile getting closer to upstream velocity. According to Figure 5 results obtained with all sgs models agree very well with the experimental data.

The comparison of rms values in the streamwise direction with experimental data is presented in Figure 7. Two peaks are observed behind the corners of the bluff body owing to high shear induced axial fluctuations. In Figure 7, some oscillations are observed in the contour plot for k-eqn and wale sgs models. The main reason for this oscillations is that relatively small data are collected for k-eqn and wale sgs models with 6 and 8.5 FTT, respectively. According to these results, it can be said that *lestr3d* accurately captures motions and turbulence in the wake region.

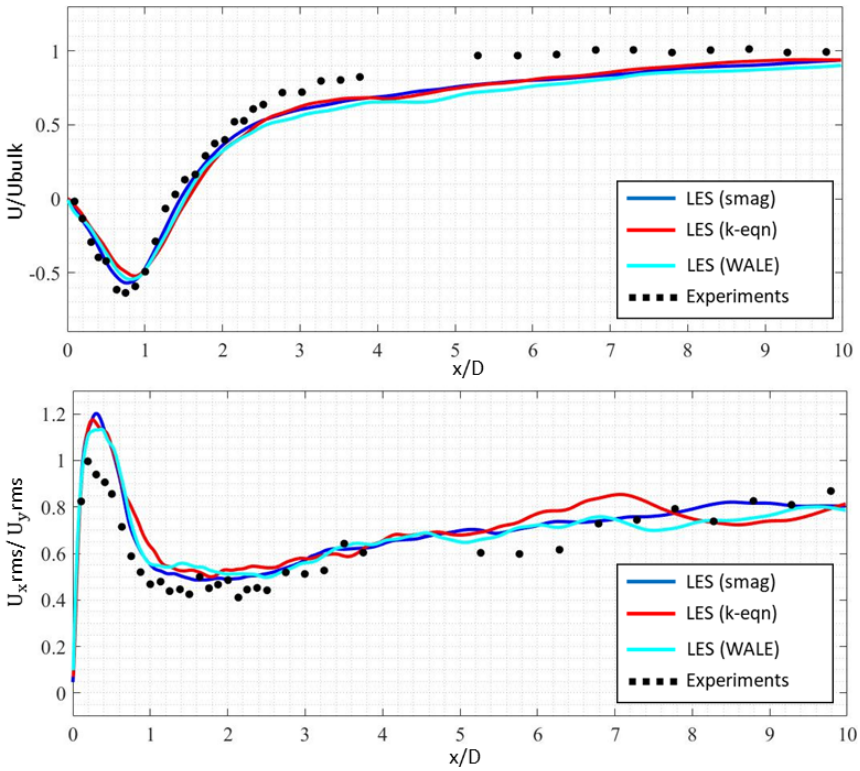

Figure 5: The mean velocity distribution (top) and the anisotropy distribution (bottom) on the centerline along the streamwise direction.

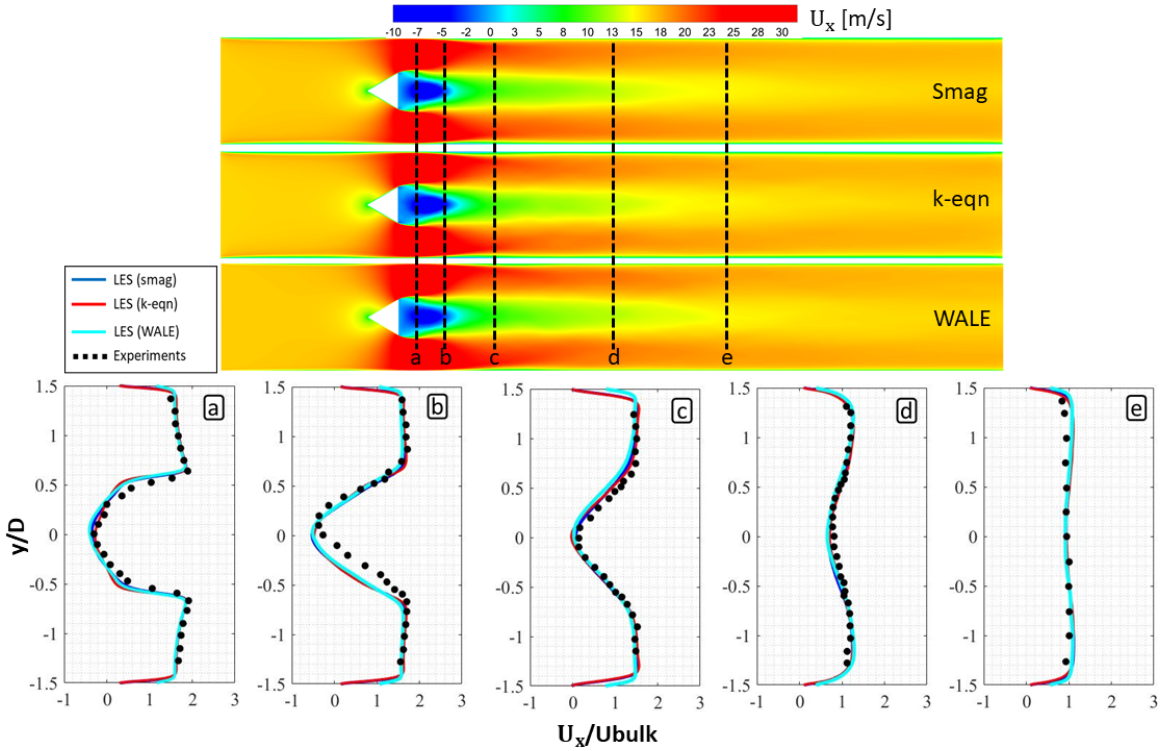

Figure 6: Top figure: mean axial velocity contours and sample lines represented as $x/D = 0.375$ (a), 0.85 (b), 1.53 (c), 3.75 (d) and 9.4 (e) stations. Bottom figure: normalized axial velocity distribution along the sample lines.

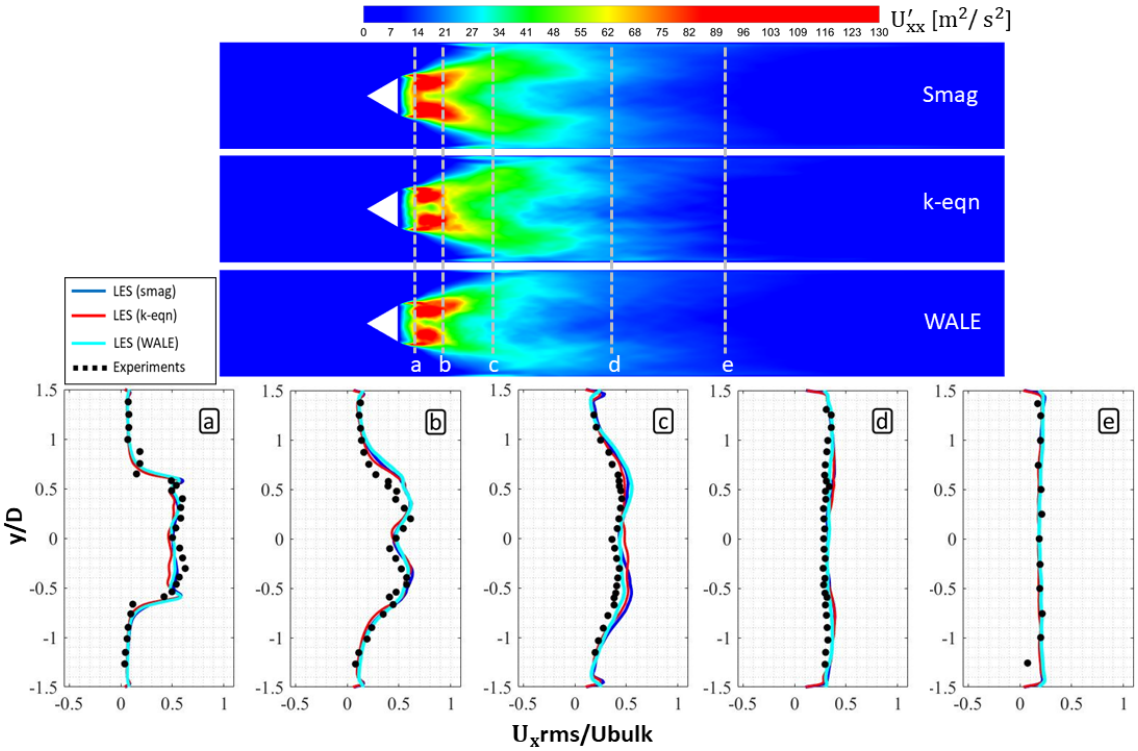

Figure 7: Top figure: rms axial velocity contours and sample lines represented as a, b, c, d, and e stations. Bottom figure: normalized axial velocity distribution along the sample lines.

All sgs models predict the flow domain correctly and show good agreement with the experimental data. It can be said that the results are independent from sgs model. The reason for this independency may be high grid resolution.

CONCLUSION

In this study, the capabilities of the in-house large eddy simulation (LES) flow solver *lestr3d* are examined by simulating a simple design with complex flow features. *lestr3d* is written in FORTRAN programming language that can run in parallel on multiple cores, can solve Navier-Stokes equations with LES approach, uses finite volume method, has different numerical methods and different sub-grid scale models.

In this investigation, cold flow of Volvo bluff body experiment is simulated because the Volvo case provides detailed measurements for validation and there is a great number of studies exist on this experiment.

In the simulations, firstly, the effect of grid resolution is investigated. It is determined that the mesh consisting of 1 million hexahedral elements do not provide sufficient accuracy and the analyzes are continued with the mesh of 4.9 million hexahedral elements. Simulations are carried out using three different sgs models: Smagorinsky, k-equation and WALE.

The shedding frequency and the Strouhal number are in good agreement with the experimental data. Furthermore, the realization of the instantaneous vorticity and Q-criterion contours clearly presents the formation and propagation of turbulent structures and wall-vortex interactions downstream of the bluff body. When the statistics in the axial direction are examined in the region behind the bluff body, it is seen that both the mean velocity values and the rms velocity values are in acceptable closeness with the experimental data for all sgs models.

ACKNOWLEDGEMENTS

This work is funded by the Scientific and Technological Research Council of Turkey (TUBITAK) under grant number 219M139 and computing resources are provided by National Center for High Performans Computing of Turkey (UHeM).

References

Andersson, N., Eriksson, L.-E. and Davidson, L. (2015) *Large-eddy simulation of subsonic jets and their radiated sound* AIAA Journal, Vol 43, No 9, p: 1-14.

Doligalski, T.L., Smith, C.R., and Walker, J.D.A.(1994) *Vortex Interactions with Walls*, Annual Review of Fluid Mechanics, Vol. 26, pp.573-616

Ecke, R., (2005). *The turbulence problem an experimentalist's perspective*, Alamos Science, Vol.29, pp.124-141

Er, S.(2019) *A finite volume based in-house large eddy simulation solver for turbulent flows in complex geometries*, Master's Thesis, Istanbul Technical University Department of Aeronautics and Astronautics Engineering.

Erlebacher, G, Hussaini, M. Y., Speziale, C. G. and Zang, T. A. (1992) *Toward the large-eddy simulation of compressible turbulent flows* J. Fluid Mech., Vol 238, p: 155-185.

Falese, M, Gicquel, L. Y. M. and Poinsot, T. (2009) *LES of bifurcation and hysteresis in confined annular swirling flows*, Computers and Fluids, Vol 89, p: 167-178.

Giacomazzi, E., Battaglia, V., and Bruno, C. (2004). *The coupling of turbulence and chemistry in a premixed bluff-body flame as studied by LES*, Combustion and Flame, Vol. 138, pp. 320-335.

Gourdain, N., Gicquel, L., Staffelbach, G., Vermorel, O., Duchaine, F., Boussuge, J.-F., and Poinsot, T. (2009) *High performance parallel computing of flows in complex geometries: II. Applications*, Computational Science & Discovery, Vol 2.

Karahan, D., T. (2017) *A new large eddy simulation solver for wall-bounded turbulent flows*, Master's Thesis, Istanbul Technical University Department of Aeronautics and Astronautics Engineering.

Karahan, D. T., Er, S., Gungor, A. G. (2017) *Large Eddy Simulation of Wall-Bounded Turbulent Flows*, Ankara International Aerospace Conference, Sep 2017.

Lacaze, G. and Oefelein, J. C. (2015) *Development of quality assessment techniques for large eddy simulation of propulsion and power systems in complex geometries*, **Technical Report**, Sandia National Laboratories.

Nicoud, F. and Ducros, F. (1999). *Subgrid-scale stress modelling based on the square of the velocity gradient tensor,*, Flow, Turbulence and Combustion, 62(1), 183–200.

Pope, S.B. (2001). *Turbulent flows*, Cambridge University Press.

Sagaut, P. (2006). *Large eddy simulation for incompressible flows*, Springer, 3rd edition.

Smagorinsky, J. (1963) *General circulation experiments with the primitive equations I. The basic experiment*, Monthly Weather Review, Vol 91,o 3, p: 99-164.

Sjunnesson, A. and Henrikson, P. and Löfström, C.(1992) *Cars measurements and visualization of reacting flows in a bluff body stabilized flame*, AIAA/ASME/SAE/ASEE 28th Joint Propulsion Conference and Exhibit, Jul 1992., AIAA - 92 - 3650.

Tennekes, H. and Lumley, J.L., (1972). *A first course in turbulence*, MIT Press.

Yoshizawa, A. and Horiuti, K. (1985). *A statistically-derived subgrid-scale kinetic energy model for the large-eddy simulation of turbulent flows*, AJournal of the Physical Society of Japan, 54(8), 2834–2839.

Wu, H., Ma, P.C., Lv, Y. and Ihme, M. (2017). *MVP-Workshop Contribution: Modeling of Volvo bluff body flame experiment*, 55th AIAA Aerospace Sciences Meeting, Grapevine, Texas, AIAA 2017-1573.